Liu *et al. Journal of Translational Medicine* (2025) 23:23
https://doi.org/10.1186/s12967-024-06038-1

Journal of
Translational Medicine

RESEARCH

Open Access

Identification of macrophage polarisation and mitochondria-related biomarkers in diabetic retinopathy

Weifeng Liu[1†], Bin Tong[1,3†], Jian Xiong[1†], Yanfang Zhu[1], Hongwei Lu[1], Haonan Xu[1], Xi Yang[1], Feifei Wang[1], Peng Yu[2*] and Yunwei Hu[1*]

Abstract

Background The activation of macrophages or microglia in patients' whole body or local eyes play significant roles in diabetic retinopathy (DR). Mitochondrial function regulates the inflammatory polarization of macrophages. Therefore, the common mechanism of mitochondrial related genes (MRGs) and macrophage polarisation related genes (MPRGs) in DR is explored in our study to illustrate the pathophysiology of DR.

Methods In this study, using common transcriptome data, differentially expressed genes (DEGs) were firstly analysed for GSE221521, while module genes related to MPRGs were obtained by weighted gene co-expression network analysis (WGCNA), intersections of DEGs with MRGs were taken, intersections of DEGs with module genes of the MPRGs were taken. After that, correlation analyses were performed to obtain candidate genes. Key genes were obtained by Mendelian randomisation (MR) analysis, then biomarkers were obtained by machine learning combined with receiver operating characteristic (ROC) and expression validation between DR and control cohorts in GSE221521 and GSE160306 to obtain biomarkers. Finally, biomarkers were subjected to immune infiltration analysis, gene set enrichment analysis (GSEA), and gene–gene interaction (GGI) analysis.

Results A number of 784 of DEGs were taken to intersect with 1136 MRGs and 782 MPRGs, respectively, after which 89 genes with correlation were taken as candidate genes. MR analysis yielded 13 key genes with clear causal links to DR. The expression trends of PTAR1 and SLC25A34 were consistent and notable between DR cohort and control cohort in GSE221521 and GSE160306. So PTAR1 and SLC25A34 were used as biomarkers. Immune infiltration analysis showed that activated NK cell and Monocyte were notably different between DR cohort and control cohorts, and PTAR1 showed the strongest positive correlations with activated NK cell. Both biomarkers were enriched in lysosome and insulin signaling pathway. The GGI network showed that biomarkers associated with prenyltransferase activity and prenylation function.

Conclusion This study identified two biomarkers (PTAR1 and SLC25A34) which explore the pathogenesis of DR and provide reference targets for drug development.

Keywords Diabetic retinopathy, Mitochondria, Macrophage polarisation, PTAR1, SLC25A34

†Weifeng Liu, Bin Tong, and Jian Xiong contributed equally to this work.

*Correspondence:
Peng Yu
yu8220182@163.com
Yunwei Hu
ndefy22085@ncu.edu.cn
Full list of author information is available at the end of the article

Introduction

Diabetic Retinopathy (DR), a disorder that impairs the retina's microvasculature and neurons, is a major culprit of vision loss [1]. The primary pathological changes in DR include pericyte loss, increased vascular permeability, neovascularization, retinal hemorrhage, and even macular edema [2]. DR comprises of an early nonproliferative and proliferative DR, which is primarily related with hyperglycemia and glucose dyscontrol [3]. Vascular endothelial growth factor (VEGF) in the retina causes leakage from nearby capillaries and promotes the formation of neovascularization, leading to retinal injury [4]. Therefore, the application of intravitreal anti-VEGF medicines like bevacizumab, ranibizumab, or aflibercept has been considered a first-line therapy in macular edema [5]. Although anti-VEGF represents a validated mechanism and demonstrates clinical efficacy, the complexity inherent in the pathogenesis of DR precludes the resolution of numerous issues through anti-VEGF treatment alone [3]. Consequently, further exploration of the underlying mechanisms is warranted.

Macrophages play an important role in regulating inflammation and maintaining tissue homeostasis. In diabetic retinas, macrophage can express TNF-α and other proinflammatory molecules [6]. Growing evidence shows that retinal inflammation, driven by hyperglycemia, is a major risk factor for DR [7]. Interleukin 1β (IL-1β), IL-18, and Tumor necrosis factor-α (TNF-α) as proinflammatory molecules has been found to be upregulated in DR [6]. A study conducted among African Americans with type 1 diabetes showed that serum pro-inflammatory factor TNFα is associated with the incidence of DR ($p < 0.001$) [8].

The regulation of macrophage adaptation and responsiveness to diverse environmental cues is attributed to cellular energy metabolism. The retina is one of the organs in the body with the highest energy consumption. Mitochondria is crucial for maintaining retinal metabolism and homeostasis [9]. Macrophages primarily produce ATP through mitochondria [10]. Under high glucose conditions, metabolic changes in retinal as well as epigenetic modifications in mitochondria-related genes can cause mitochondrial dysfunction and induce apoptosis. Furthermore, mitophagy and mitochondrial dynamics undergo adaptive changes [11]. Certain molecules situated in the mitochondria of inflammatory macrophages play a significant role in modulating mitochondrial dynamics and oxidative respiration, thereby affecting macrophage polarization [12]. Therefore, investigating the role of mitochondria in macrophages during the development and progression of DR may offer new insights for preventing and treating DR.

This study, based on transcriptomics data from public databases, employed DEGs and WGCNA analysis to identify macrophage polarization-related genes (MPRGs) and mitochondrial-related genes. Subsequently, MR analysis and machine learning were used to screen biomarkers linked to both macrophage polarization and mitochondria in DR, and explored their causal relationships. Systematic analyses, including PPI, GGI, GSEA, and immune cells analysis were conducted to uncover the biological mechanisms of these biomarkers involved in DR, confirming the accuracy and biological significance of the screening results. This provides valuable insights for further exploration of DR pathogenesis and offers potential reference targets for drug development.

Materials and methods

Data source

Two transcriptomic datasets of Diabetic Retinopathy (DR) from Gene Expression Omnibus (GEO) database (https://www.ncbi.nlm.nih.gov/geo/) were encompassed in this study. We employed GSE221521 as the training set and GSE160306 as the validation set. GSE221521 (GPL24676 platform) consisted of blood from 69 DR samples and 50 control samples [13], which utilized high-throughput sequencing. GSE160306 (GPL20301 platform) included blood from 20 DR samples and 20 control samples, which utilized chip sequence.

A total of 1,136 mitochondrial related genes (MRGs) from MitoCarta3.0 database (http: //www.broadinstitute.org/mitocarta) [14]. A total of 35 macrophage polarization related genes (MPRGs) from literature [15].

The Genome-Wide Association Studies (GWAS) data of expression Quantitative Trait Loci (eQTL) of candidate genes was searched from Integrative Epidemiology Unit (IEU) open GWAS database (https://gwas.mrcieu.ac.uk/). To see more details in Supplementary Table 8. Searching DR dataset using Diabetic Retinopathy as keyword from IEU open GWAS database to obtain finn_b_DM_RETINOPATHY dataset, which had 16,380,459 single nucleotide polymorphisms (SNPs) from 216,666 samples (DR: 14,584, Control: 202,082) were European.

Differential expression analysis

The DESeq2 package (v 1.42.0) [16] was utilized for differential expressed analysis in GSE221521 dataset ($|\log_2$Fold Change (FC)$| > 0.5$ and adj.$P < 0.05$). The ggplot2 package (v 3.5.1) [17] was employed to show the result of differentially expressed genes (DEGs) in the top 10.

Weighted gene co-expression network analysis (WGCNA)

Firstly, the GSVA package (v 1.50.0) [18] was employed to analyze MPRGs single-sample gene set enrichment analysis (ssGSEA) scores between DR group and control

group in GSE221521 dataset ($p < 0.05$). MPRGs scores was used as traits for WGCNA. The WGCNA package (v 1.72–5) [19] was employed to identify module genes that were highly correlated with Hierarchical clustering of all samples (height = 200), using the euclidean distance of the sample expression profiles was utilized to identify and exclude outliers. Subsequently, R2 = 0.8 and connectivity was close to 0 were utilized to screen for soft thresholds (β). Gene adjacency was then calculated, which led to computing gene similarity, from which a gene dissimilarity coefficient was derived to create a hierarchical clustering tree of genes. The minimum gene count per module was set to 100 and shear height was 0.4 according to the standards of the dynamic tree cutting algorithm. Then, key modules were identified by calculating the correlations between module and phenotypic traits (correlation (|cor|) > 0.3, $p < 0.05$). Further screening of module genes by Gene Significance (GS) and Module Membership (MM) metrics can be utilized to identify genes of high significance in the module (GS > 0.3, MM > 0.5).

Screening and enrichment analysis of candidate genes

The VennDiagram package (v 1.7.3) [20]was employed to take intersections for DEGs and MRGs, then obtained DE-MRGs. On the other hand, taking intersections for DEGs and modular genes, then obtained DE-MPRGs. Then the psych package (v 2.2.5) [20]was employed to analyze the Spearman between DE-MRGs and DE-MPRGs. Candidate genes were selected based on their correlation with related genes (|r| > 0.3 and $p < 0.05$). Finally, the result was showed in heatmap. Functional enrichment of these candidate genes based on kyoto encyclopedia of genes and genomes (KEGG) and gene ontology (GO) databases using the clusterProfiler package (v 4.10.1) [21](p.adj < 0.05). The Search Tool for the Retrieval of Interacting Genes (STRING) database (https://string-db.org) was employed to build the protein–protein interaction (PPI) network of candidate genes (confidence = 0.4), and Cytoscape software (v 3.7.1) [22] was employed to visualise the PPI network.

Mendelian randomization (MR) analysis

Candidate genes as exposure factors and DR as outcome event. Three basic premises underlie MR studies: (1) a robust and notable correlation existed between instrumental variables (IVs) and exposure; (2) IVs were unrelated to confounding factors; (3) It was only affected by exposure factors and not directly related to outcomes. The extract_instruments function of TwoSampleMR package (v 0.6.4) [23] was employed to obtain exposure factors and screen IVs. Looking for notably related IVs ($p < 5 \times 10^{-6}$) of exposure factors, IVs with Linkage Disequilibrium (LD) were removed using the three metrics, clump = TRUE, $R^2 = 0.001$, and kb = 10. Then extract_outcome_data function was employed to perform ending readings and screen IVs, the screening indicators of IVs were proxies was TRUE and rsq was 0.8, this was followed by screening for instrumental variables that were associated with exposure factors but not with outcomes. Harmonisation of effect alleles and effect sizes through the TwoSampleMR package function harmonise_data. Subsequently, the IVs was calculated to be F statistic, F < 10 for single nucleotide polymorphism (SNP) and eliminate weak IVs. Then, MR combined 5 algorithms for MR analysis, which were MR-Egger [24], Weighted median [25], Inverse variance weighted (IVW) [26], Simple mode [23] and Weighted mode [27]. The IVW method served as the primary measure for determining statistical significance ($p < 0.05$), the odds ratio (OR) > 1 was considered as a risk factor, and OR < 1 was considered as a protective factor. Then correlation analysis was carried out with scatter plot, forest plot, and randomness analysis with funnel plot. Sensitivity analysis was performed to verify the results of MR. Initially, heterogeneity was assessed using the mr_heterogeneity function, and an innotable result ($p > 0.05$) indicating the absence of notable heterogeneity [28]. Furthermore, the mr_pleiotropy_test function and mr_presso function were employed to scrutinize the potential for horizontal pleiotropy ($p > 0.05$) [29]. The robustness of the results was additionally ascertained through Leave-One-Out (LOO) analysis. This approach iteratively omitted individual SNPs to verify the stability of the causal estimates in the absence of single variants [30], finally, the Steiger directional test was applied to eliminate the prospect of reverse causation. The evidence of a one-way causal association was strengthened when the correct causal direction outcome was confirmed as TRUE and the steiger ($p < 0.05$) [31]. Eventually, the candidate genes causally linked to DR were obtained through MR analysis, which were recorded as key genes.

Recognition of candidate feature genes by machine learning algorithm

In the GSE221521, the Boruta package (v 8.0.0) [32] was used to perform a Boruta analysis on key genes. In this analysis, the genes were ranked based on their importance, which were selected as feature gene 1. Key genes previously identified were used to construct a support vector machines-recursive feature elimination (SVM-RFE) model, the model was employed to rank the importance of each candidate biomarkers, identifying the optimal combination with the lowest error rate. Subsequently, the caret package (v 6.0–94) [33] was employed to obtain feature genes 2 for SVM-RFE. Finally, the feature genes obtained from the above two machine learning methods were intersected using the

VennDiagram package (v 1.7.3) to obtain candidate candidate biomarkers.

Identification of biomarkers

The pROC package (v 1.18.5) [34] was utilized to plot receiver operating characteristic (ROC) curves in both GSE221521 and GSE160306 to assess the ability of candidate biomarkers to differentiate between DR group and control group, with area under curve (AUC) values being calculated. A gene demonstrating an AUC exceeding 0.7 indicated a strong capability to discriminate between sample types. Genes with AUC > 0.7 were used as candidate biomarkers for subsequent analysis in GSE221521 and GSE160306. In addition, the expression trends of these candidate biomarkers were evaluated between LPR and control cohorts within GSE221521 and GSE160306. Genes that exhibited consistent expression trends in GSE221521 and GSE160306 and notable differences between DR and control cohorts were defined as biomarkers. Box plots were used show the expression of these biomarkers ($p < 0.05$).

Construction of nomogram

In order to see the diagnostic value of biomarkers, building nomogram via rms package (v 6.5.0) [35] to verify the effectiveness of the model. In order to assess clinical predictive models, diagnostic tests and biomarkers, building decision curve. In order to estimate the clinical effect of the nomogram more visually, the AUC of ROC curve was calculated by pROC package (v 1.18.5).

Immune infiltration

The enrichment of 22 immune cell types in DR and control cohorts from GSE221521 dataset were assessed and the CIBERSORT algorithm was utilized (v 1.03) [36]. Additionally, the distinctions in the enrichment of immune cell infiltration in DR cohorts and control cohorts were analyzed ($p < 0.05$). Moreover, the relationship between differential immune cells, and connection between biomarkers and differential immune cells in GSE221521 dataset samples were analyzed using psych package (v 2.2.5) [37].

The gene set enrichment analysis (GSEA) of key genes

The c2.cp.kegg.v7.4.symbols.gmt as the reference gene set, which was downloaded from molecular signatures database (MSigDB) (https://www.gsea-msigdb.org/gsea/msigdb) ($p < 0.05$). The clusterProfiler package (v 4.10.1) [21] was employed to calculate the relevance score between the biomarkers and the other genes in each sample separately, then followed by GSEA ($p < 0.05$), The pathway of biomarkers were shown in the top 5 and in descending order in line graph.

Chromosomal localisation and tissue expression analysis of biomarkers and RNA methylation modifications

In order to download gene location information from the ENSEMBL database (https://grch37.ensembl.org/index.html), RCircos package(v 1.2.2) [38] was used to analyze specific location of biomarkers on chromosomes. Subsequently, biomarkers were analysed in the Human Protein Atlas (HPA) database (https://www.proteinatlas.org) for their specific expression in tissues and cells. To understand RNA methylation modifications of biomarkers, sequence-based RNA adenosine methylation site predictor (SRAMP) (http://www.cuilab.cn/sramp/) predicted m6A modification sites of biomarkers and their location in RNA secondary structure.

Gene–gene interaction (GGI) network construction and molecular regulatory network

GeneMANIA (http://www.genemania.org) database was employed to search for interacting genes with the biomarkers and construct a gene interaction GGI network. For molecular regulatory networks and the pathways involved, based on biomarkers, miRNAs obtained from miRDB database (https://mirdb.org/) and TargetScan database (https://www.targetscan.org/vert_80/) were taken for intersection. The starbase database (https://starbase.sysu.edu.cn/) was then employed to obtain key lncRNAs upstream of the targeted intersecting miRNAs and filter the targeted IncRNAs based on clipExpNum > 4. Then, the ChEA3 database (https://maayanlab.cloud/chea3/) was utilized to predict biomarker transcription factors (TFs) and select the top 40 TFs in terms of scores, and Cytoscape software (v 3.7.1) was used to visualise TFs-biomarker network. Finally, the multiMiR package (v 0.98.0.2) [39] was employed to investigate the lncRNA-miRNA-mRNA network of the biomarkers and visualized them using the galluvial package (v 0.12.5) [40].

Statistical analysis

All analyses were executed in R language (v 4.2.2). Differences between groups were analyzed by Wilcoxon test. $p < 0.05$ was considered statistically notable.

Results

Screening of DEGs and modular genes

The GSE221521 dataset obtained 784 DEGs (492 DEGs were up-regulated and 292 DEGs were down-regulated) between DR group and control group (Fig. 1A). On the other hand, the MPRGs score was notably higher in the DR group than in the control group in GSE221521 ($p < 0.05$) (Fig. 1B). Analysed by WGCNA, Hierarchical clustering analysis revealed there was 1 outlier sample and excluded it (Fig. 1C). When a soft threshold β of 12

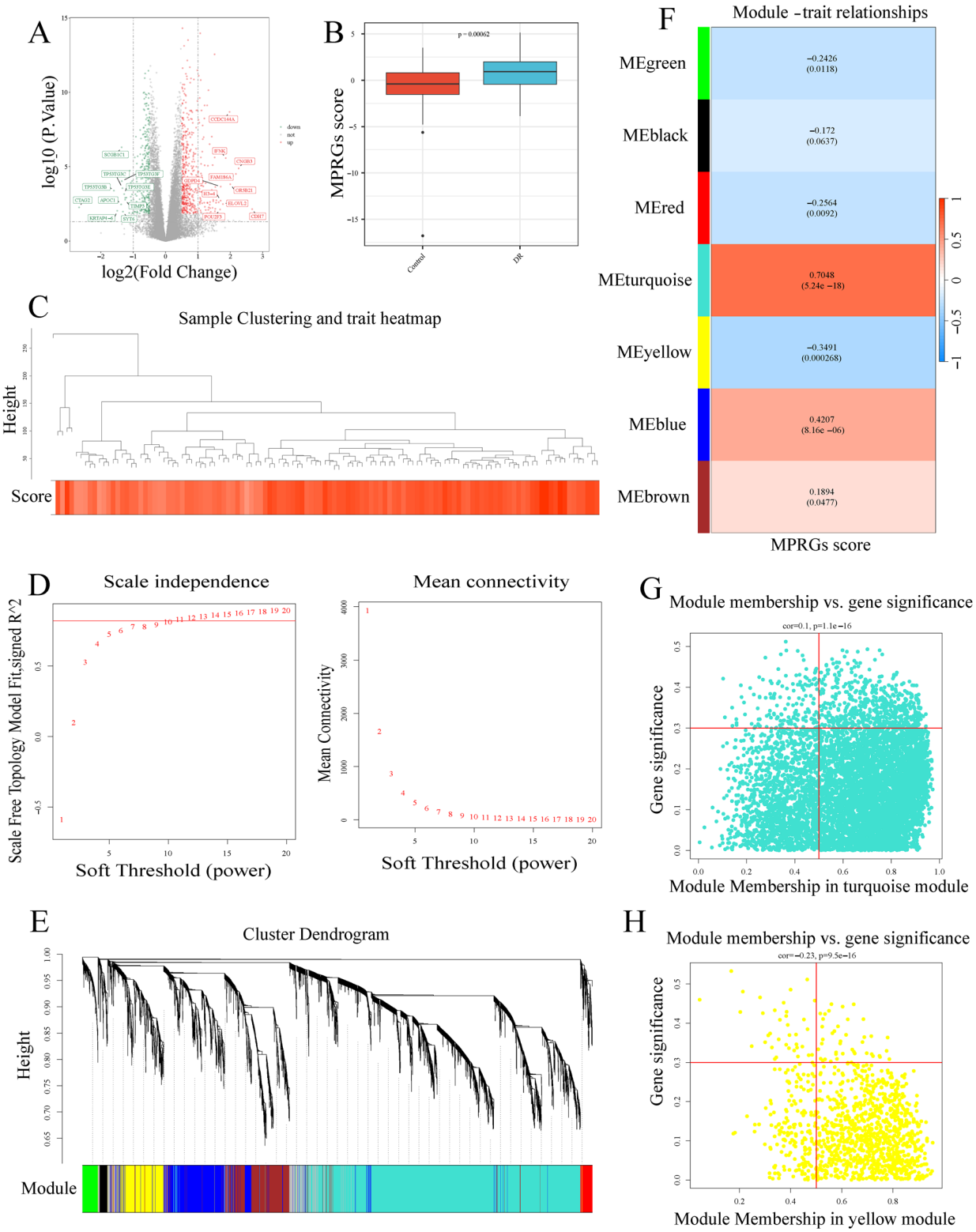

Fig. 1 Screening of DEGs and modular genes. **A** Volcano plot of 784 differentially expressed genes in DR. **B** Macrophage polarisation related genes score was notably higher in the DR group than in the control group in GSE221521 ($p < 0.05$) **C** Hierarchical clustering of DR samples revealed 1 outlier sample and excluded it. **D** Determining the optimal soft threshold β of 12. **E** Construction of gene co-expression network, aggregated 7 modules were. **F** Heatmap of the correlation between modules and MPRGs scores. **G** Scatter plot of gene-module membership in the blue-green module. **H** Scatter plot of gene-module membership in the yellow module

was chosen, the network approximated a scale-free distribution (Fig. 1D). After determining the soft threshold, the construction of the co-expression network was carried out, and 7 modules were aggregated (Fig. 1E). In the non-grey module, the p-value < 0.05 and correlation with this a scores |cor| > 0.3. Identifying the key modules we obtained the MEturquoise and MEyellown modules. One of the modules most notably associated with MPRGs scores was the MEturquoise (cor = 0.7048, $p = 5.24 \times 10^{-18}$), which contained 7,423 genes. On the other hand, The highest negative correlation was for the MEyellown (cor = − 0.3491, $p = 2.68 \times 10^{-4}$), which contained 1,191 genes. (Fig. 1F). In total, 8,614 module genes were obtained. A total of 782 modular genes were obtained between GS and MM in highly notable correlation (Fig. 1G, H).

The crucial biological pathways and PPI networks of candidate genes

A total of 26 DE-MRGs were obtained from the intersection of 784 DEGs and 1,136 MRGs and 63 DE-MPRGs were obtained from the intersection of 784 DEGs and 782 modular genes (Fig. 2A, B). Finally, 88 genes were obtained as candidate genes by Spearman correlation analysis (|r| > 0.3 and $p < 0.05$) (Fig. 2C). GO pathway analysis of 88 candidate genes led to the identification of 211 biological process (BP) entries. While 32 cellular components (CC) entries, as well as 52 molecular functions (MF) entries were found. The GO pathway including mitochondrial inner membrane, ribosome, mitophagy, negative regulation of protein localization and regulation of intracellular protein transport, unfolded protein binding (Fig. 2D, Supplementary Table 5). Furthermore, 4 KEGG pathways were identified, which were ribosome, RNA polymerase, mitophagy animal and nucleotide excision repair (Fig. 2E). PPI network which consists of 34 proteins and 45 edges, RPS11 and RSC1A1 had more connections and interactions with other proteins (Fig. 2F).

Acquisition of key genes

A two-sample MR analysis was performed with 88 candidate genes as exposure factors and DR as the outcome. A number of 13 genes were identified by IVW and were used as key genes ($p < 0.05$). As a result, 6 protective factors were obtained: RPL28, RPL36, ATP5F1E, PRPF31, PET100, SEPTIN4 (OR < 1, $p < 0.05$), while the PTAR1, CYP27A1, SLC4A8, SLC25A34, FGD6, LDHD, GAN genes were risk factors (OR > 1, $p < 0.05$) (Fig. 3A). Analyzing the correlation between exposure factors and outcomes in scatter plot, PTAR1, CYP27A1, SLC4A8, SLC25A34, FGD6, LDHD and GAN genes were positively correlated, while the RPL28, RPL36, ATP5F1E, PRPF31, PET100 and SEPTIN4 genes were negatively correlated (Supplementary Fig. 1). Forest plots showed that the effect value of RPL28, RPL36, ATP5F1E, PRPF31, PET100 and SEPTIN4 were less than 0, the effect value of PTAR1, CYP27A1, SLC4A8, SLC25A34, FGD6, LDHD and GAN genes were great than 0 (Supplementary Fig. 2). SNP numbers were largely symmetrical on both sides of the IVW line and consistent with Mendel's second law (Supplementary Fig. 3). Sensitivity analyses of the 13 exposure factors and outcomes yielded 13 exposure factors for no heterogeneity ($p > 0.05$) (Supplementary Table 1), and there were no horizontal pleiotropy existed between 13 exposure factors and outcome ($p > 0.05$) (Supplementary Table 2, 3). In LOO, there were no points of no serious bias, and the reliability of the results was illustrated (Supplementary Fig. 4). At last, DR was used as exposure factor and the 13 genes as outcome in the steiger test for reverse causality, the directional relationship was judged to be "TRUE", and there was no reverse causality between the 13 exposure factors and the outcome ($p < 0.05$) (Supplementary Table 4). Finally, RPL28, RPL36, ATP5F1E, PRPF31, PET100, SEPTIN4, PTAR1, CYP27A1, SLC4A8, SLC25A34, FGD6, LDHD, GAN were recorded as key genes.

Establishment of PTAR1 and SLC25A34 as biomarkers for DR

To further recognize biomarkers, 13 key genes were included in both SVM and Boruta analyses. In the Boruta algorithm, resulting in the identification of 11 candidate biomarkers (Fig. 3B). Within the SVM-RFE, screening of 13 genes yielded 11 candidate biomarkers (Fig. 3C). Then, by overlapping these two sets of candidate biomarkers, SLC25A34、GAN、RPL36、FGD6、PTAR1、PRPF31、SLC4A8、ATP5F1E、PET100、CYP27A1 were identified as candidate biomarkers (Fig. 3D). Subsequently, ROC curves were plotted for these 10 candidate biomarkers in both GSE221521 and GSE160306 to assess their ability to differentiate between DR and control cohorts. Then 2 candidate biomarkers were selected in the two groups (AUC ≥ 0.7), which were PTAR1 and SLC25A34 (Fig. 3E, F). In GSE221521 and GSE160306 dataset, PTAR1, SLC25A34 expression trends were consistent and notable, and both were notably up-regulated in DR (Fig. 3G, H). Therefore, PTAR1 and SLC25A34 were recorded as biomarkers for subsequent analyses.

PTAR1 and SLC25A34 nomogram diagnostics in DR

In the GSE221521, PTAR1 and SLC25A34 were found to have better diagnostic ability for DR by nomogram (Fig. 4A). The net benefit of nomogram was higher than the other individual factor, indicating that nomogram had the best predictions (Fig. 4B). The area under the

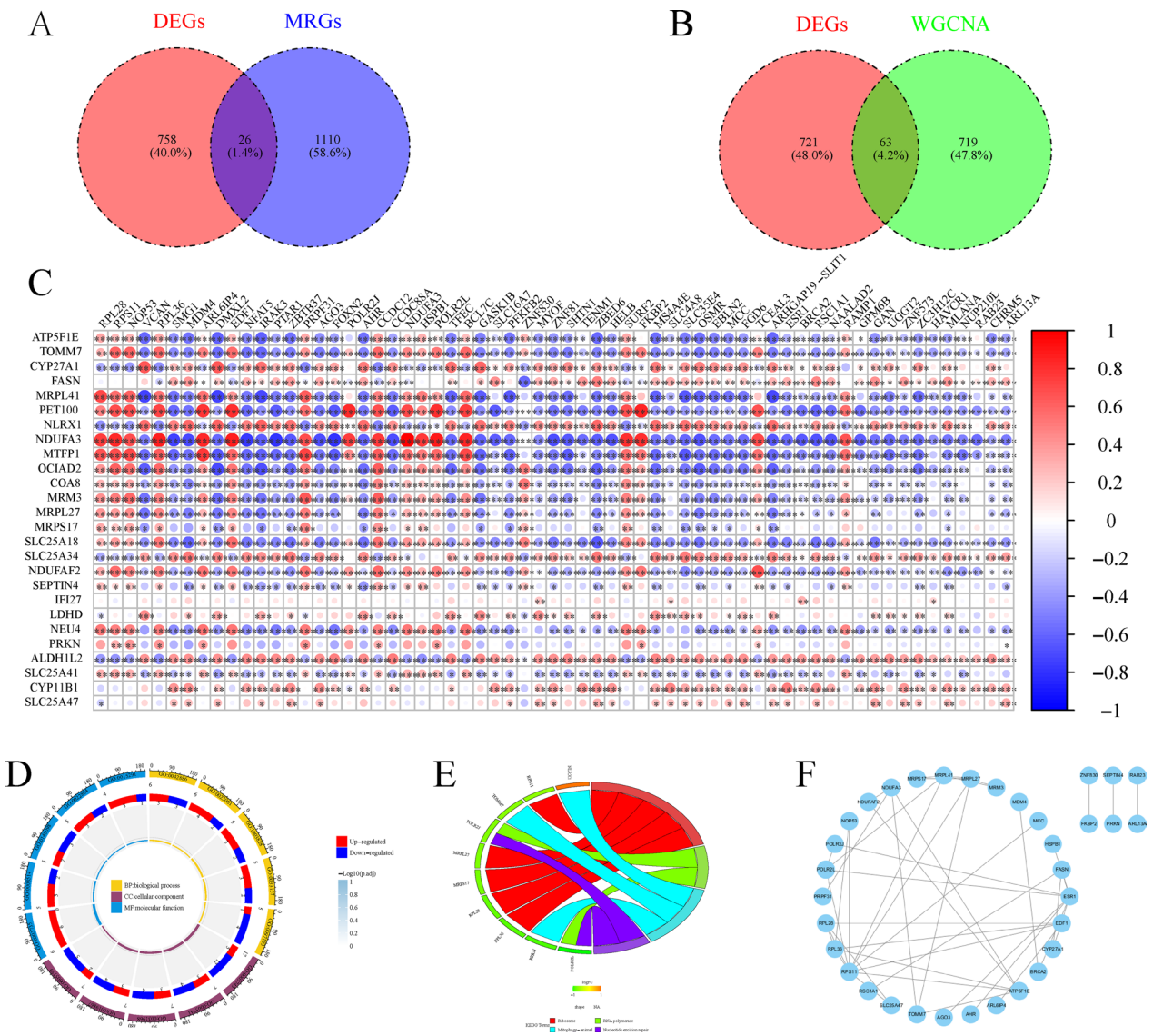

Fig. 2 The crucial biological pathways and PPI networks for candidate genes. **A** 26 DE-MRGs were obtained from Venn diagram of 784 DEGs and 1,136 MRGs. **B** 63 DE-MPRGs were obtained from Venn diagram of 784 DEGs and 782 WGCNA module genes. **C** 88 genes were obtained as candidate genes by Spearman correlation analysis of DE-MRGs and DE-MPRGs. **D** Circular plot of GO enrichment for candidate genes. **E** KEGG pathway diagram for candidate genes. **F** PPI network for candidate genes

curve AUC of the nomogram model were 0.745, indicating that it was a good reliability of prediction model for DR occurrence (Fig. 4C).

Analysis and correlation of immune cells

The results of the infiltration of 22 immune cells were displayed in the Fig. 4D. Immune cells were first filtered based on the 22 immune cells whose expression was 0 in 75% of the samples, 13 of immune cells (naive B cell, memory B cell, CD8 + T cell, CD4 + memory resting T cell, CD4 + memory activated Tcell, follicular helper T cell, regulatory (Tregs) T cell, resting NK cell, activated NK cell, Monocyte, M2 Macrophage, activated Mast cell, and Neutrophil) were obtained, activated NK cell and Monocyte were notably different between DR cohort and control cohort ($p < 0.05$), and activated NK cell was notable upregulated in control cohort, but Monocyte was notable upregulated in DR cohort. (Fig. 4E). Thereafter, correlations between these immune cells and biomarkers revealed that PTAR1 (cor = − 0.41, $p = 3.96 \times 10^{-6}$) showed the strongest positive correlations with activated NK cell. (Fig. 4F).

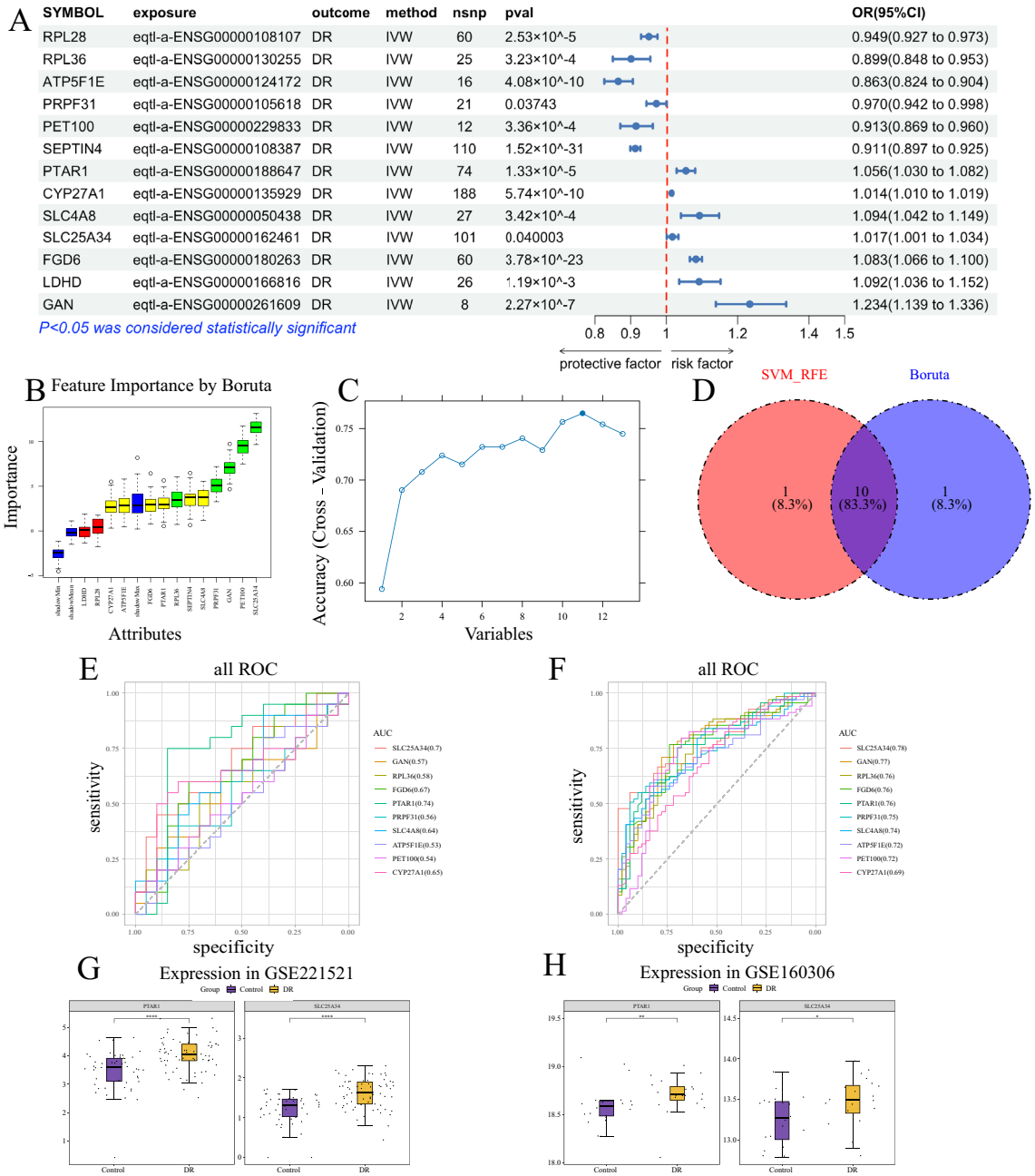

Fig. 3 Establishment of PTAR1 and SLC25A34 as biomarkers for DR. **A** MR results of 13 key genes. **B** Boruta analysis for 13 genes identified 11 candidate biomarkers. **C** SVM-RFE analysis for 13 genes identified 11 candidate biomarkers. **D** Venn diagram for Boruta analysis and SVM-RFE analysis identified 10 candidate biomarkers. **E** ROC curve of candidate biomarkers in GSE221521 identified PTAR1 and SLC25A34 as biomarkers. **F** ROC curve for candidate biomarkers in GSE160306. **G** Expression levels of PTAR1 and SLC25A34 in GSE221521. **H** Expression levels of PTAR1 and SLC25A34 in GSE160306

The gene set enrichment analysis (GSEA) of key genes

We employed GSEA to explore the pathways which biomarkers influence DR development. In GSE221521 dataset ($p < 0.05$), SLC25A34 was mainly enriched to 58 KEGG pathways. These pathways include protein synthesis processes like Ribosome, neurodegenerative diseases such as Parkinson's disease, as well as the NOTCH, and Insulin signaling pathway (Fig. 4G). PTAR1 was mainly enriched to 19 KEGG pathways. These pathways include Phosphatidylinositol, Neurotrophin, ERBB,

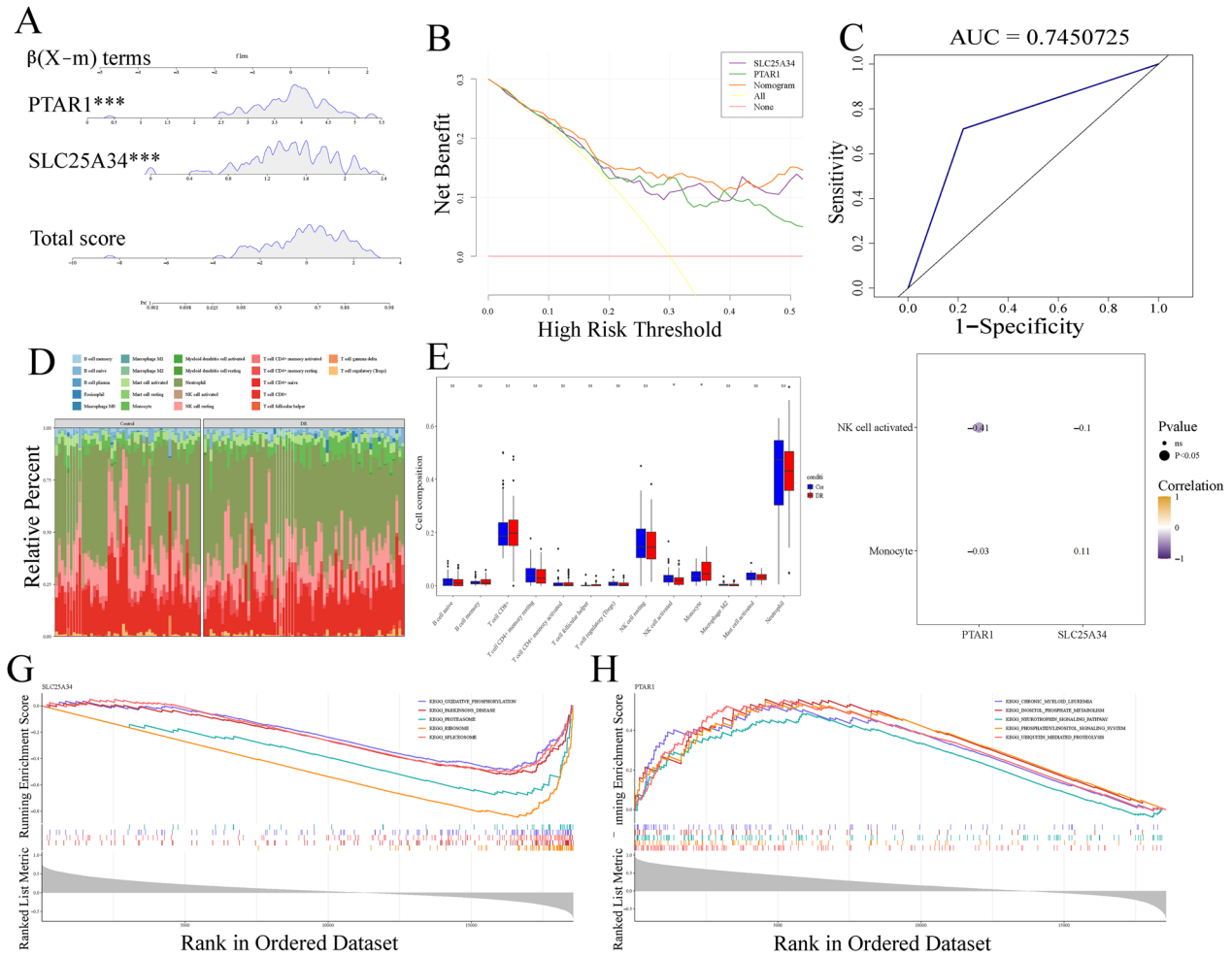

Fig. 4 Nomogram diagnostics, immune cells analysis and GSEA analysis of PTAR1 and SLC25A34. **A** Nomogram of PTAR1 and SLC25A34 found PTAR1 and SLC25A34 have better diagnostic ability for DR. **B** Decision Curve Analysis of the nomogram found nomogram had the best predictions. **C** ROC curve of the nomogram indicated that it was a good reliability of prediction model for DR occurrence. **D** Immune cell infiltration between DR and control groups obtained 13 immune cells. **E** Differences in immune cells between DR and control groups. **F** Correlation between biomarkers and different immune cells. **G** GSEA of SLC25A34. **H** GSEA of PTAR1

Toll-like receptor, Insulin signaling pathway. SLC25A34 and PTAR1 are both involved in the Lysosomal pathway and Insulin signaling pathway (Fig. 4H). PTAR1 and SLC25A34 are both engaged in the Lysosomal pathway and Insulin signaling pathways. (Supplementary tables 6, 7).

The expression of SLC25A34 and PTAR1 in different tissues

Firstly, the chromosomal location analysis was performed for biomarkers, SLC25A34 gene on chromosome 9 and PTAR1 gene on chromosome 1 (Fig. 5A). To understand the expression of biomarkers in skin tissues and cells, PTAR1 was enriched in tissues, and the top five tissues that express it were bone marrow, thymus, parathyroid, kidney and liver (Fig. 5D). Moreover, SLC25A34 had the highest expression content in tongue, followed by skeletal muscle, duodenum, small intestine and so on (Fig. 5E). To further understand RNA methylation modification of biomarkers, the prediction of SLC25A34 m6A locus was performed at the position of highest confidence (1461) (Fig. 5F), while the prediction of PTAR1 m6A locus was performed at the position of highest confidence (824) (Fig. 5G). The predicted structures of SLC25A34 and PTAR1 secondary structure m6A loci were then shown in Fig. 5B, C.

The network construction analysis of SLC25A34 and PTAR1

The GGI network showed that biomarkers associated with prenyltransferase activity and prenylation function (Fig. 6A).The miRNAs obtained from miRDB database

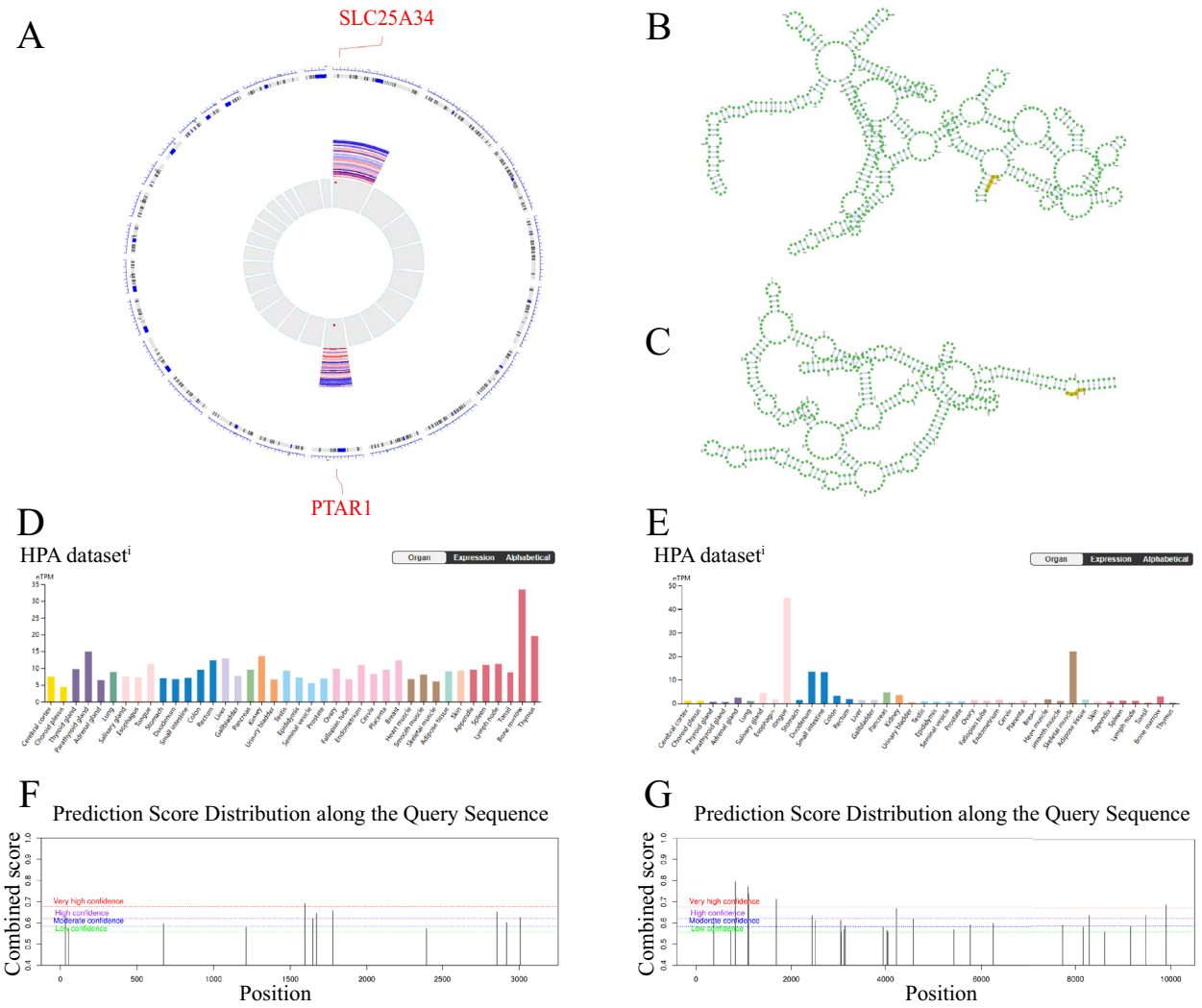

Fig. 5 The expression of SLC25A34 and PTAR1 in different tissues. **A** Chromosomal localization revealed SLC25A34 gene on chromosome 9 and PTAR1 gene on chromosome 1. **B** predicted structures of SLC25A34 secondary structure m6A loci. **C** predicted structures of PTAR1 secondary structure m6A loci. **D** Expression of PTAR1 in different human tissues. **E** Expression of SLC25A34 in different human tissues. **F** prediction of SLC25A34 m6A locus. **G** Prediction of PTAR1 m6A locus

and TargetScan database were taken to intersect to get 23 upstream miRNAs related to biomarkers and 17 lncRNA (Fig. 6B, C). After that, to understand the regulatory relationship between transcription factors (TFs) and biomarkers, in which there were 12 TFs regulating SLC25A34, while there were 28 TFs regulating PTAR1, including 42 nodes and 40 edges (Fig. 6D).

Discussion

Between 1990 and 2020, DR was the mainly cause of blindness with an increasing global age-standardized prevalence [41]. It is estimated that by 2040, the number of people with diabetes worldwide will exceed 640 million [42], and as the lifespan of diabetic patients continues to increase, the number of people with DR and resulting vision impairment is expected to rise rapidly [41]. The activation of macrophages or microglia in patients' whole body or local eyes play significant roles in DR [7]. Macrophages are responsible for homeostasis and host defense. They are present all over the eye, such as in the cornea, iris, ciliary body, retina, choroid and sclera [43]. Evidence shows that the activation, polarization, and function of macrophages are key points in the inflammatory reaction caused by diabetes [44]. Hyperglycemia triggers the aggregation of macrophages/microglia with the M1 phenotype [43]. A large number of studies have demonstrated that macrophage-mediated inflammation is vital in DR and precedes the activation of

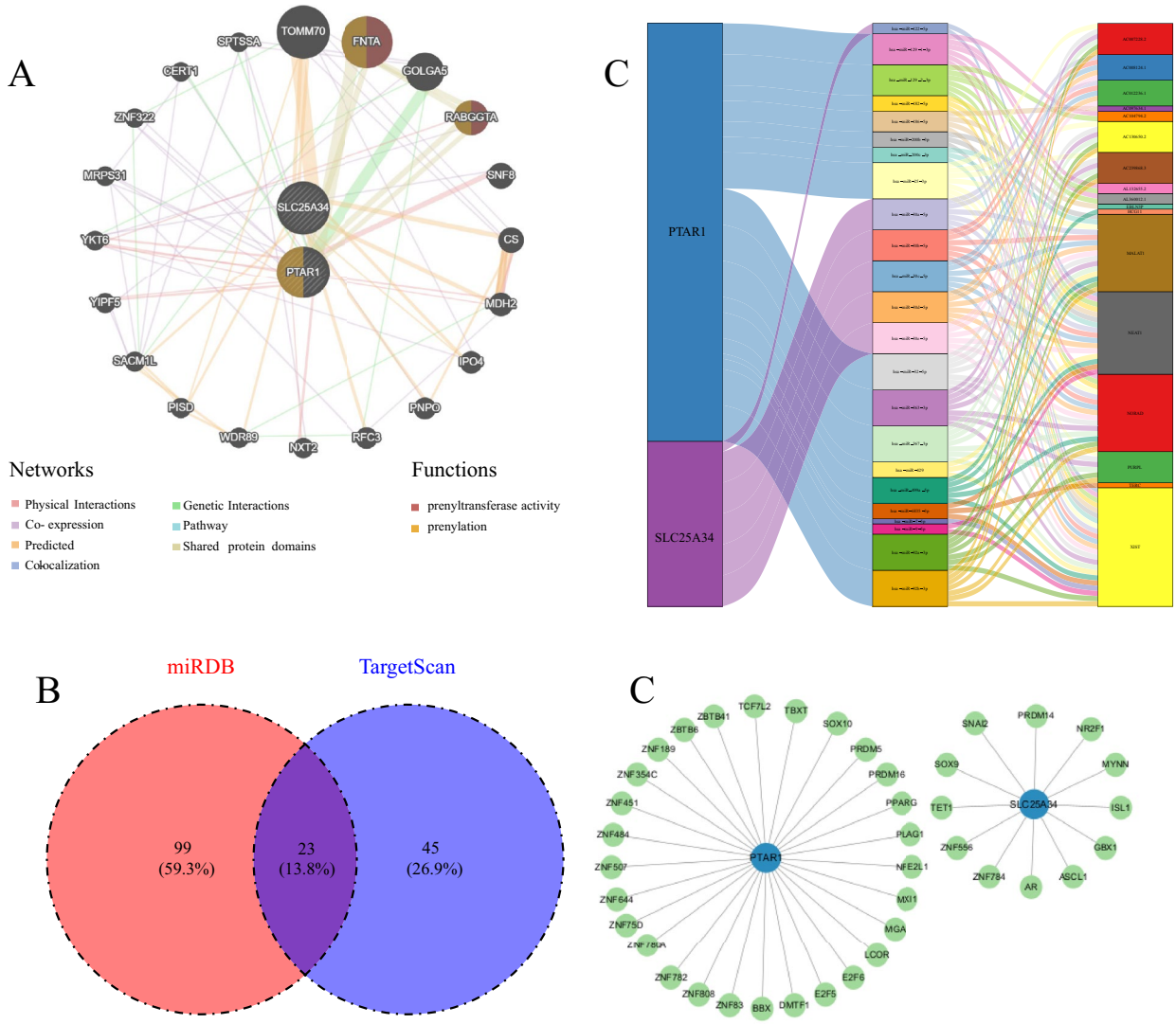

Fig. 6 The network construction analysis of SLC25A34 and PTAR1. **A** GGI network of SLC25A34 and PTAR1 showed that biomarkers associated with prenyltransferase activity and prenylation function. **B** Venn diagram of miRNAs obtained from the miRDB and TargetScan databases. **C** lncRNA-miRNA-mRNA network. **D** TFs-mRNA network

other glial cells and neuronal apoptosis [45]. Mitochondrial function regulates the inflammatory polarization of macrophages [12]. For examplethe translocator protein (18 kDa) (TSPO) is a transmembrane protein of the outer mitochondrial membrane and is essential for mitochondrial cholesterol translocation [43, 46]. Moreover, TSPO is highly expressed in macrophages and microglia [47]. Similarly, SIRT6 is crucial for macrophage activation [48] and mitochondrial function regulation [49]. Recently, SIRT6 has been found to be associated with the occurrence and development of DR. High blood glucose leads to increased VEGF, decreased BDNF, and reduced SIRT6 protein level in the retina. Importantly, the retinal layers of specific Sirt6 knockout mice are thinner [50]. Therefore, the common mechanism of mitochondrial related genes (MRGs) and macrophage polarisation related genes (MPRGs) in DR is explored in our study to illustrate the pathophysiology of DR.

In this study, differential expression gene (DEGs) analysis was first performed on the training set, identifying 784 differentially expressed genes. Simultaneously, WGCNA analysis was used to screen MPRGs-related candidate genes. The intersection of DEGs with MRGs and MPRGs was taken, and genes with a correlation coefficient ($|r| > 0.3$) and $p < 0.05$ in the intersecting gene set were selected as candidate

genes, resulting in 88 candidate genes. Functional analyses, such as GO and KEGG enrichment, were conducted on these candidate genes. We found that these genes are related to ribosomes, RNA polymerase, nucleotide excision repair, protein localization and transport, the mitochondrial inner membrane, and mitophagy. This suggests that changes in energy supply, protein synthesis, localization, and transport may occur in DR, potentially affecting retinal structure and function and worsening pathological changes. And this change is influenced by both mitochondrial function and macrophage activity. Abnormal protein expression has already been detected in the tears and vitreous fluid of DR patients [51, 52]. Certain molecules situated in the mitochondria of inflammatory macrophages was found to play a significant role in modulating mitochondrial dynamics and oxidative respiration, thereby affecting macrophage polarization [12]. We also found that these genes are associated with unfolded protein binding. Vascular degeneration, a key pathological change in DR, precedes proliferative retinopathy. This underscores the critical role of neovascularization in DR progression. Many studies show that when endothelial cells encounter angiogenic stimuli, such as oxidative stress and inflammation, the unfolded protein response is activated and is crucial for endothelial cell survival and function [53]. Therefore, we hypothesis that mitochondrial dysfunction may lead to insufficient energy supply, affecting normal macrophage functions such as phagocytosis and antigen presentation. It may also indirectly regulate macrophage inflammatory responses and immune modulation by impacting processes like protein synthesis, folding, transport, and localization. However, elevated oxidative stress in the retina and its capillary cells during DR is detected prior to mitochondrial dysfunction and the acceleration of apoptosis [54]. Therefore, further research is required to substantiate this debate.

Mendelian randomization (MR) uses genetic variants as instrumental variables, minimizing confounding factors and reverse causality, which enables a more precise evaluation of the causal link between the candidate genes and DR. MR analysis identified 13 genes with significant causal relationships for further analysis. Using machine learning algorithms, including Boruta and SVM-RFE analysis, 10 candidate feature genes were selected for subsequent analysis. ROC curve analysis was performed on the training and validation sets, showing that the AUC values of PTAR1 and SLC25A34 were both greater than 0.7, indicating strong diagnostic capabilities in distinguishing between disease and control samples. Expression validation confirmed consistent and significant trends for these two genes, leading to their selection as biomarkers for further investigation.

PTAR1 is the newly identified α-subunit of GGTase3, playing a critical role in protein prenylation [55]. Approximately 300 proteins in the human proteome are modified by prenyltransferases, many of which are essential for cellular functions such as membrane transport, signal transduction, apoptosis, and cell cycle regulation. Notably, some oncogenic proteins rely on prenylation for activation, making the inhibition of prenylation a proposed strategy for cancer treatment [56]. GGTase3 geranylgeranylates FBXL2, directing it to the cell membrane, where it facilitates the polyubiquitination of anchored proteins [55]. FBXL2 is a pro-survival gene whose product, activated by mitogens, inhibits apoptosis by activating the PI3K-AKT pathway and preventing mitochondrial calcium overload [57]. The binding of FBXL2 to GGTase3 is entirely facilitated by PTAR1, which completely covers concave surface of the F-box protein [55].

SLC25A34 (Solute Carrier Family 25 Member 34) is part of the solute carrier family 25 (SLC25), whose proteins are primarily responsible for transporting nutrients like ATP, ADP, and phosphate across the mitochondrial inner membrane [58]. This process is essential for energy conversion and maintaining cellular function. These proteins undergo significant conformational changes, enabling them to transport large biochemical compounds without substantial proton leakage [58]. The clinical manifestations of mitochondrial diseases vary across different tissues and cell types but often involve energy-demanding organs such as the brain and retina. The SLC25 family plays a key role in various physiological processes, including cellular metabolism, energy supply, and apoptosis. Recent studies have shown that abnormal expression of SLC25 family members may be linked to the development and progression of tumors and metabolic disturbance [59].

Immune cell infiltration characteristics were assessed to evaluate the impact of the systemic immune system on DR. We found that monocytes were significantly upregulated, while activated NK cells were significantly downregulated in the DR cohort. Thereafter, correlations between these immune cells and biomarkers revealed that PTAR1 ($cor = -0.41$, $p = 3.96 \times 10^{-6}$) showed the strongest positive correlation with activated NK cells. Upregulation of monocytes and downregulation of NK cells were also observed in STZ-induced DR mouse models [60]. NK cells are a vital type of lymphocyte in the human immune system, playing a key role in innate immunity. Their cytotoxic activity is not restricted by MHC and does not depend on antibodies, making them crucial for antitumor, antiviral, and immune regulatory responses [61]. Monocytes, derived from hematopoietic

stem cells in the bone marrow, are the largest blood cells and the largest white blood cells by volume. They play a critical role in both acute and chronic inflammation, tissue repair, and immune regulation [61]. However, the mechanisms by which these two cell types contribute to the development and progression of DR still require further investigation.

Using GSEA, we investigated the pathways through which biomarkers impact DR progression. In GSE221521 dataset, SLC25A34 was mainly enriched to 58 KEGG pathways. These pathways include protein synthesis processes like Ribosome, neurodegenerative diseases such as Parkinson's disease, as well as the NOTCH, and Insulin signaling pathway. PTAR1 was mainly enriched to 19 KEGG pathways. These pathways include Phosphatidylinositol, Neurotrophin, ERBB, Toll-like receptor, Insulin signaling pathway. SLC25A34 and PTAR1 are both involved in the Lysosomal pathway and Insulin signaling pathway. Our findings are consistent with previous studies. First, lysosomal impairment and autophagy disruption are among the initial factors in DR development, driving neovascularization, endothelial damage. Elevated glucose induces autophagy, but lysosomal dysfunction results in p62/SQTSM1 buildup, which triggers excessive VEGF secretion and causes retinal Müller cell death [62]. Second, insulin stimulates the absorption, storage and convertion of carbohydrates, fatty acids, and amino acids. Both neuron vascular cells in the retina express insulin receptors, and are insulin-sensitive tissue. Dysfunction in Insulin signaling can lead to cellular dysfunction and death in retinal diseases [63]. Third, neovascularization is one of the main pathological features in DR. NOTCH/VEGFR regulation leads to differential dynamics of VE-cadherin junctions, driving functional rearrangements of vascular endothelial cells during sprouting [64], and abnormalities in the NOTCH/VEGFR signaling pathway may exacerbate DR. Then, phosphatidylinositol 3 kinase (PI3K)/AKT signaling pathway is activated by hyperglycemia, which induces the expression of fibronectin and laminin, leading to the formation of fibrotic membranes in DR progression [65]. In addition, neurotrophin receptors may be engaged in the development of epiretinal membranes (ERM), potentially contributing to proliferative diabetic retinopathy [66]. Consistent with our findings, the ErbB signaling pathway has also been found to be associated with DR [67]. Moreover, upregulation of TLR4 mRNA and protein expression was observed in the STZ-induced DR rat model. Additionally, the protein levels of downstream signaling molecules of TLR4 were significantly elevated [68]. In another study, researchers observed a significant increase in retinal tissue thickness, a biomarker of retinal damage severity, in STZ-induced TLR4 knockout diabetic mice [69]. Therefore, SLC25A34 and PTAR1 may involve in the development of DR through these pathways, but further experiments are needed to confirm this.

However, this study has some limitations. Firstly, this study should be further validated in well-powered studies. Future studies will incorporate more experimental data and different types of datasets to further verify and improve the current research results. In addition, prospective studies should be carried out in combination with clinical data to further validate the mechanism in DR. Secondly, since all participants in our MR study were of European ancestry, the risk of false associations due to population stratification bias was minimized. However, this restricts the applicability of our findings to populations outside of European descent.

Conclusions

This study, based on general transcriptomic data, utilized Mendelian randomization (MR) and bioinformatics methods to investigate the mechanisms of mitochondrial-related genes (MRGs) and macrophage polarization-related genes (MPRGs) in diabetic retinopathy (DR), focusing on their involvement in biological functions. It identified PTAR1 and SLC25A34 as biomarkers associated with both mitochondrial function and macrophage polarization in DR. It contributes to further exploration of the pathogenesis of DR and provides potential target references for drug development.

Supplementary Information

The online version contains supplementary material available at https://doi.org/10.1186/s12967-024-06038-1.

Additional file 1.

Additional file 2.

Acknowledgements

We thank the authors and participants in all of the GWASs we used for sharing their findings publically available.

Author contributions

W.L., B.T., P.Y. and Y.H. conceptualized and designed the study. W.L., B.T., and J.X. performed the statistical analyses. Y.Z. and H.L. were responsible for data visualization. H.X., X.Y. and F.W. contributed to data acquisition and analysis. B.T. and W.L. wrote the initial draft of the manuscript. All authors critically reviewed, revised and approved the final version of the manuscript. Y.H. and P.Y. contributed to the conception and study design, drafting the text, and preparing the figures as the corresponding authors.

Funding

Natural Science Foundation of Jiangxi Province (No. 20224BAB216049 to YW.H), National Natural Science Foundation of China (No. 82360204 to YW.H), and Innovation Training Program for College Students in Nanchang University (No. 2024CX289 to B.T).

Availability of data and materials
The original contributions presented in the study are included in the article/Supplementary Table. Further inquiries can be directed to the corresponding authors.

Declarations

Ethics approval and consent to participate
Specific ethical approval was not required for this study because all data were obtained from sources available to the public.

Consent for publication
Not appliable.

Competing interests
The authors declare that they have no competing interests.

Author details
[1]Ophthalmic Center, The Second Affiliated Hospital, Jiangxi Medical College, Nanchang University, Nanchang 330006, Jiangxi, China. [2]Department of Endocrinology and Metabolism, The Second Affiliated Hospital, Jiangxi Medical College, Nanchang University, Nanchang 330006, Jiangxi, China. [3]School of Ophthalmology and Optometry, Jiangxi Medical College, Nanchang University, Nanchang 330006, Jiangxi, China.

Received: 17 October 2024 Accepted: 25 December 2024
Published online: 06 January 2025

References

1. Wong TY, Cheung CM, Larsen M, Sharma S, Simó R. Diabetic retinopathy. Nat Rev Dis Primers. 2016;2:16012.
2. Gardner TW, Antonetti DA. Novel potential mechanisms for diabetic macular edema: leveraging new investigational approaches. Curr Diab Rep. 2008;8:263–9.
3. Gangwani RA, Lian JX, McGhee SM, Wong D, Li KK. Diabetic retinopathy screening: global and local perspective. Hong Kong Med J. 2016;22:486–95.
4. Penn JS, Madan A, Caldwell RB, Bartoli M, Caldwell RW, Hartnett ME. Vascular endothelial growth factor in eye disease. Prog Retin Eye Res. 2008;27:331–71.
5. Wells JA, Glassman AR, Ayala AR, Jampol LM, Aiello LP, Antoszyk AN, Arnold-Bush B, Baker CW, Bressler NM, Browning DJ, et al. Aflibercept, bevacizumab, or ranibizumab for diabetic macular edema. N Engl J Med. 2015;372:1193–203.
6. Yang LP, Sun HL, Wu LM, Guo XJ, Dou HL, Tso MO, Zhao L, Li SM. Baicalein reduces inflammatory process in a rodent model of diabetic retinopathy. Invest Ophthalmol Vis Sci. 2009;50:2319–27.
7. Lee R, Wong TY, Sabanayagam C. Epidemiology of diabetic retinopathy, diabetic macular edema and related vision loss. Eye Vis (Lond). 2015;2:17.
8. Roy MS, Janal MN, Crosby J, Donnelly R. Inflammatory biomarkers and progression of diabetic retinopathy in African Americans with type 1 diabetes. Invest Ophthalmol Vis Sci. 2013;54:5471–80.
9. Jiménez-Loygorri JI, Benítez-Fernández R, Viedma-Poyatos Á, Zapata-Muñoz J, Villarejo-Zori B, Gómez-Sintes R, Boya P. Mitophagy in the retina: viewing mitochondrial homeostasis through a new lens. Prog Retin Eye Res. 2023;96: 101205.
10. Van den Bossche J, O'Neill LA, Menon D. Macrophage immunometabolism: where are we (going)? Trends Immunol. 2017;38:395–406.
11. Wu Y, Zou H. Research progress on mitochondrial dysfunction in diabetic retinopathy. Antioxidants (Basel). 2022;11:2250.
12. Dowling JK, Afzal R, Gearing LJ, Cervantes-Silva MP, Annett S, Davis GM, De Santi C, Assmann N, Dettmer K, Gough DJ, et al. Mitochondrial arginase-2 is essential for IL-10 metabolic reprogramming of inflammatory macrophages. Nat Commun. 2021;12:1460.
13. Xiang ZY, Chen SL, Qin XR, Lin SL, Xu Y, Lu LN, Zou HD. Changes and related factors of blood CCN1 levels in diabetic patients. Front Endocrinol (Lausanne). 2023;14:1131993.
14. Gu Y, Yu W, Qi M, Hu J, Jin Q, Wang X, Wang C, Chen Y, Yuan W. Identification and validation of hub genes and pathways associated with mitochondrial dysfunction in hypertrophy of ligamentum flavum. Front Genet. 2023;14:1117416.
15. Zhao Y, Li M, Yang Y, Wu T, Huang Q, Wu Q, Ren C. Identification of macrophage polarization-related genes as biomarkers of chronic obstructive pulmonary disease based on bioinformatics analyses. Biomed Res Int. 2021;2021:9921012.
16. Love MI, Huber W, Anders S. Moderated estimation of fold change and dispersion for RNA-seq data with DESeq2. Genome Biol. 2014;15:550.
17. Gustavsson EK, Zhang D, Reynolds RH, Garcia-Ruiz S, Ryten M. ggtranscript: an R package for the visualization and interpretation of transcript isoforms using ggplot2. Bioinformatics. 2022;38:3844–6.
18. Hänzelmann S, Castelo R, Guinney J. GSVA: gene set variation analysis for microarray and RNA-seq data. BMC Bioinformatics. 2013;14:7.
19. Langfelder P, Horvath S. WGCNA: an R package for weighted correlation network analysis. BMC Bioinformatics. 2008;9:559.
20. Chen H, Boutros PC. VennDiagram: a package for the generation of highly-customizable Venn and Euler diagrams in R. BMC Bioinformatics. 2011;12:35.
21. Wu T, Hu E, Xu S, Chen M, Guo P, Dai Z, Feng T, Zhou L, Tang W, Zhan L, et al. clusterProfiler 4.0: a universal enrichment tool for interpreting omics data. Innovation (Camb). 2021;2:100141.
22. Liu P, Xu H, Shi Y, Deng L, Chen X. Potential molecular mechanisms of plantain in the treatment of gout and hyperuricemia based on network pharmacology. Evid Based Complement Alternat Med. 2020;2020:3023127.
23. Hemani G, Zheng J, Elsworth B, Wade KH, Haberland V, Baird D, Laurin C, Burgess S, Bowden J, Langdon R, et al. The MR-Base platform supports systematic causal inference across the human phenome. Elife. 2018;7:e34408.
24. Bowden J, Davey Smith G, Burgess S. Mendelian randomization with invalid instruments: effect estimation and bias detection through Egger regression. Int J Epidemiol. 2015;44:512–25.
25. Bowden J, Davey Smith G, Haycock PC, Burgess S. Consistent estimation in mendelian randomization with some invalid instruments using a weighted median estimator. Genet Epidemiol. 2016;40:304–14.
26. Burgess S, Scott RA, Timpson NJ, Davey Smith G, Thompson SG. Using published data in Mendelian randomization: a blueprint for efficient identification of causal risk factors. Eur J Epidemiol. 2015;30:543–52.
27. Hartwig FP, Davey Smith G, Bowden J. Robust inference in summary data Mendelian randomization via the zero modal pleiotropy assumption. Int J Epidemiol. 2017;46:1985–98.
28. Qin Q, Zhao L, Ren A, Li W, Ma R, Peng Q, Luo S. Systemic lupus erythematosus is causally associated with hypothyroidism, but not hyperthyroidism: a Mendelian randomization study. Front Immunol. 2023;14:1125415.
29. Davey Smith G, Hemani G. Mendelian randomization: genetic anchors for causal inference in epidemiological studies. Hum Mol Genet. 2014;23:R89-98.
30. Cui Z, Feng H, He B, He J, Tian Y. Relationship between serum amino acid levels and bone mineral density: a Mendelian randomization study. Front Endocrinol (Lausanne). 2021;12: 763538.
31. Xiao G, He Q, Liu L, Zhang T, Zhou M, Li X, Chen Y, Chen Y, Qin C. Causality of genetically determined metabolites on anxiety disorders: a two-sample Mendelian randomization study. J Transl Med. 2022;20:475.
32. Yue S, Li S, Huang X, Liu J, Hou X, Zhao Y, Niu D, Wang Y, Tan W, Wu J. Machine learning for the prediction of acute kidney injury in patients with sepsis. J Transl Med. 2022;20:215.
33. Zhang Z, Zhao Y, Canes A, Steinberg D, Lyashevska O. Predictive analytics with gradient boosting in clinical medicine. Ann Transl Med. 2019;7:152.
34. Robin X, Turck N, Hainard A, Tiberti N, Lisacek F, Sanchez JC, Müller M. pROC: an open-source package for R and S+ to analyze and compare ROC curves. BMC Bioinformatics. 2011;12:77.
35. Sachs MC. plotROC: a tool for plotting ROC curves. J Stat Softw. 2017;79:2.
36. Newman AM, Liu CL, Green MR, Gentles AJ, Feng W, Xu Y, Hoang CD, Diehn M, Alizadeh AA. Robust enumeration of cell subsets from tissue expression profiles. Nat Methods. 2015;12:453–7.
37. Orifjon S, Jammatov J, Sousa C, Barros R, Vasconcelos O, Rodrigues P. Translation and adaptation of the adult developmental coordination disorder/dyspraxia checklist (ADC) into Asian Uzbekistan. Sports (Basel). 2023;11:135.

38. Zhang H, Meltzer P, Davis S. RCircos: an R package for Circos 2D track plots. BMC Bioinformatics. 2013;14:244.
39. Ru Y, Kechris KJ, Tabakoff B, Hoffman P, Radcliffe RA, Bowler R, Mahaffey S, Rossi S, Calin GA, Bemis L, Theodorescu D. The multiMiR R package and database: integration of microRNA-target interactions along with their disease and drug associations. Nucleic Acids Res. 2014;42: e133.
40. Brunson JC. ggalluvial: layered grammar for alluvial plots. J Open Source Softw. 2017;2020:5.
41. Steinmetz JD, Bourne RR, Briant PS, Flaxman SR, Taylor HR, Jonas JB, Abdoli AA, Abrha WA, Abualhasan A, Abu-Gharbieh EG, Adal TG. Causes of blindness and vision impairment in 2020 and trends over 30 years, and prevalence of avoidable blindness in relation to VISION 2020: the right to sight: an analysis for the Global Burden of Disease Study. Lancet Glob Health. 2021;9:e144–60.
42. Ogurtsova K, da Rocha Fernandes JD, Huang Y, Linnenkamp U, Guariguata L, Cho NH, Cavan D, Shaw JE, Makaroff LE. IDF diabetes atlas: global estimates for the prevalence of diabetes for 2015 and 2040. Diabetes Res Clin Pract. 2017;128:40–50.
43. Chen P, Ding N, Pan D, Chen X, Li S, Luo Y, Chen Z, Xu Y, Zhu X, Wang K, Zou W. PET imaging for the early evaluation of ocular inflammation in diabetic rats by using [(18)F]-DPA-714. Exp Eye Res. 2024;245: 109986.
44. Kinuthia UM, Wolf A, Langmann T. Microglia and inflammatory responses in diabetic retinopathy. Front Immunol. 2020;11: 564077.
45. Park YG, Lee JY, Kim C, Park YH. Early microglial changes associated with diabetic retinopathy in rats with streptozotocin-induced diabetes. J Diabetes Res. 2021;2021:4920937.
46. Zhou Y, Ou Y, Ju Z, Zhang X, Zheng L, Li J, Sun Y, Liu X. Visualization of translocator protein (18 kDa) (TSPO) in the retina of diabetic retinopathy rats using fluorine-18-DPA-714. Ann Nucl Med. 2020;34:675–81.
47. MacAskill MG, Stadulyte A, Williams L, Morgan TEF, Sloan NL, Alcaide-Corral CJ, Walton T, Wimberley C, McKenzie CA, Spath N, et al. Quantification of macrophage-driven inflammation during myocardial infarction with (18)F-LW223, a novel TSPO Radiotracer with binding independent of the rs6971 human polymorphism. J Nucl Med. 2021;62:536–44.
48. Zou Y, Zhang J, Xu J, Fu L, Xu Y, Wang X, Li Z, Zhu L, Sun H, Zheng H, Guo J. SIRT6 inhibition delays peripheral nerve recovery by suppressing migration, phagocytosis and M2-polarization of macrophages. Cell Biosci. 2021;11:210.
49. Smirnov D, Eremenko E, Stein D, Kaluski S, Jasinska W, Cosentino C, Martinez-Pastor B, Brotman Y, Mostoslavsky R, Khrameeva E, Toiber D. SIRT6 is a key regulator of mitochondrial function in the brain. Cell Death Dis. 2023;14:35.
50. Zorrilla-Zubilete MA, Yeste A, Quintana FJ, Toiber D, Mostoslavsky R, Silberman DM. Epigenetic control of early neurodegenerative events in diabetic retinopathy by the histone deacetylase SIRT6. J Neurochem. 2018;144:128–38.
51. Hernández C, Segura RM, Fonollosa A, Carrasco E, Francisco G, Simó R. Interleukin-8, monocyte chemoattractant protein-1 and IL-10 in the vitreous fluid of patients with proliferative diabetic retinopathy. Diabet Med. 2005;22:719–22.
52. Ghosh S, Ghosh S, Azharuddin M, Bera S, Datta H, Dasgupta A. Change in tear protein profile in diabetic retinopathy with duration of diabetes. Diabetes Metab Syndr. 2014;8:233–5.
53. Zhang SX, Ma JH, Bhatta M, Fliesler SJ, Wang JJ. The unfolded protein response in retinal vascular diseases: implications and therapeutic potential beyond protein folding. Prog Retin Eye Res. 2015;45:111–31.
54. Kowluru RA, Kowluru A, Veluthakal R, Mohammad G, Syed I, Santos JM, Mishra M. TIAM1-RAC1 signalling axis-mediated activation of NADPH oxidase-2 initiates mitochondrial damage in the development of diabetic retinopathy. Diabetologia. 2014;57:1047–56.
55. Kuchay S, Wang H, Marzio A, Jain K, Homer H, Fehrenbacher N, Philips MR, Zheng N, Pagano M. GGTase3 is a newly identified geranylgeranyltransferase targeting a ubiquitin ligase. Nat Struct Mol Biol. 2019;26:628–36.
56. Hougland JL, Fierke CA. Getting a handle on protein prenylation. Nat Chem Biol. 2009;5:197–8.
57. Kuchay S, Duan S, Schenkein E, Peschiaroli A, Saraf A, Florens L, Washburn MP, Pagano M. FBXL2- and PTPL1-mediated degradation of p110-free p85β regulatory subunit controls the PI(3)K signalling cascade. Nat Cell Biol. 2013;15:472–80.
58. Ruprecht JJ, Kunji ERS. The SLC25 mitochondrial carrier family: structure and mechanism. Trends Biochem Sci. 2020;45:244–58.
59. Roy N, Alencastro F, Roseman BA, Wilson SR, Delgado ER, May MC, Bhushan B, Bello FM, Jurczak MJ, Shiva S, et al. Dysregulation of lipid and glucose homeostasis in hepatocyte-specific SLC25A34 knockout mice. Am J Pathol. 2022;192:1259–81.
60. Suvas P, Liu L, Rao P, Steinle JJ, Suvas S. Systemic alterations in leukocyte subsets and the protective role of NKT cells in the mouse model of diabetic retinopathy. Exp Eye Res. 2020;200: 108203.
61. Soderquest K, Powell N, Luci C, van Rooijen N, Hidalgo A, Geissmann F, Walzer T, Lord GM, Martín-Fontecha A. Monocytes control natural killer cell differentiation to effector phenotypes. Blood. 2011;117:4511–8.
62. de Lopes Faria JM, Duarte DA, Montemurro C, Papadimitriou A, Consonni SR, de Lopes Faria JB. Defective autophagy in diabetic retinopathy. Invest Ophthalmol Vis Sci. 2016;57:4356–66.
63. Reiter CE, Gardner TW. Functions of insulin and insulin receptor signaling in retina: possible implications for diabetic retinopathy. Prog Retin Eye Res. 2003;22:545–62.
64. Bentley K, Franco CA, Philippides A, Blanco R, Dierkes M, Gebala V, Stanchi F, Jones M, Aspalter IM, Cagna G, et al. The role of differential VE-cadherin dynamics in cell rearrangement during angiogenesis. Nat Cell Biol. 2014;16:309–21.
65. Qin D, Zhang GM, Xu X, Wang LY. The PI3K/Akt signaling pathway mediates the high glucose-induced expression of extracellular matrix molecules in human retinal pigment epithelial cells. J Diabetes Res. 2015;2015: 920280.
66. Harada T, Harada C, Mitamura Y, Akazawa C, Ohtsuka K, Ohno S, Takeuchi S, Wada K. Neurotrophic factor receptors in epiretinal membranes after human diabetic retinopathy. Diabetes Care. 2002;25:1060–5.
67. He K, Lv W, Zhang Q, Wang Y, Tao L, Liu D. Gene set enrichment analysis of pathways and transcription factors associated with diabetic retinopathy using a microarray dataset. Int J Mol Med. 2015;36:103–12.
68. Wang YL, Wang K, Yu SJ, Li Q, Li N, Lin PY, Li MM, Guo JY. Association of the TLR4 signaling pathway in the retina of streptozotocin-induced diabetic rats. Graefes Arch Clin Exp Ophthalmol. 2015;253:389–98.
69. Fu H, Liu H. Deletion of toll-like receptor 4 ameliorates diabetic retinopathy in mice. Arch Physiol Biochem. 2023;129:519–25.

Publisher's Note